Desalination and Water Treatment
www.deswater.com

doi: 10.5004/dwt.2017.20748

75 (2017) 245–252
May

Synthesis of nanoadsorbent and modeling of dye removal from wastewater using adaptive neuro-fuzzy inference system

Niyaz Mohammad Mahmoodi*, Zahra Hosseinabadi-Farahani, Hooman Chamani

Department of Environmental Research, Institute for Color Science and Technology, Tehran, Iran, Tel. +98 21 22969771; Fax: +98 21 22947537; emails: mahmoodi@icrc.ac.ir, nm_mahmoodi@aut.ac.ir, nm_mahmoodi@yahoo.com (N.M. Mahmoodi), zahrahof80@gmail.com (Z. Hosseinabadi-Farahani), chamani.hooman@yahoo.com (H. Chamani)

Received 27 August 2016; Accepted 21 March 2017

ABSTRACT

In this paper, $CuMnO_2$ nanomaterial was synthesized and its dye removal ability was studied. The characteristics of the synthesized nanomaterial were investigated using Fourier transform infrared, scanning electron microscopy and X-ray diffraction. Adaptive neuro-fuzzy inference system (ANFIS) was applied for modeling of dye removal from colored wastewater. The effect of adsorbent dosage and dye concentration on dye removal was studied. Dye removal process followed pseudo-second-order model and Langmuir isotherm. Furthermore, good agreement between values of predicted and experimental dye removal percentage was observed. The results showed that ANFIS could effectively predict the behavior of the process.

Keywords: $CuMnO_2$ nanomaterial; Synthesis; ANFIS modeling; Dye removal; Kinetics; Isotherm

1. Introduction

Human health and ecosystem are affected by pollutants. The presence of pesticides, radionuclides, heavy toxic metal ions and dyes in the aquatic environment has caused a critical environmental problem [1–9]. Dyes as organic materials are widely used in various industries including cosmetics, leather, textiles, plastics, etc. The presence of low concentration of dyes in aqueous environment is highly visible and undesirable. Approximately 10%–15% amount of the dyes is not used during the dyeing process and released into wastewater [10–13]. Basic dyes have been classified as toxic colorants. Therefore, improved or cost-effective technologies are required for removal of these dyes from textile effluents [14]. Dye removal from water and wastewater is a difficult process due to its complex structure and non-biodegradability [15]. Several processes such as coagulation, membrane filtration, adsorption, photocatalysis, advance oxidation, etc., have been studied to treat colored wastewater [16,17]. Dye destruction by biological process is a time consuming and low efficiency method because dyes have high chemical stability. In addition, some dye degradation by-products are more toxic and carcinogenic than their parental molecules for aquatic organisms [18–22]. However, adsorption does not leave behind any toxic intermediates or by-products [23]. Furthermore, adsorption is a suitable choice for wastewater treatment due to its design simplicity, ease of operation and insensitivity to toxic substances [24,25]. The adsorption is a mass transfer process which can be defined as accumulation of material at the interface of two phases [26]. Various organic and inorganic adsorbents were studied. An easy and inexpensive synthesis method of the adsorbent is one of the most important factors for selecting a suitable adsorbent [27,28]. Recently, there has been considerable research interest in studying adsorption behaviors of organic dye molecules on the surface of inorganic nanomaterial.

In this work, $CuMnO_2$ nanomaterial was synthesized using a low cost and simple method and used as an adsorbent for removal of cationic dyes (Basic Blue 41: BB41 and Basic Red 18: BR18) from aqueous solution. Adaptive

* Corresponding author.

neuro-fuzzy inference system (ANFIS) was applied for modeling of dye removal from colored wastewater. The adsorbent was characterized using Fourier transform infrared (FTIR), scanning electron microscopy (SEM) and X-ray diffraction (XRD). The effect of operational parameters (adsorbent dosage and dye concentration) on dye removal was evaluated. The kinetics and isotherm of dye adsorption were studied in detail.

2. Materials and methods

2.1. Materials

BB41 and BR18 were used as cationic dyes. The chemical structure of dyes is shown in Fig. 1. Other chemicals including copper sulfate, manganese nitrate and sodium hydroxide pellet were obtained from Merck (Germany). All materials were used without further purification.

2.2. Synthesis of $CuMnO_2$ nanomaterial

An alkaline solution was prepared by dissolving sodium hydroxide (1 g) pellet in 90 mL deionized water. Manganese nitrate tetrahydrate (1 g) and copper sulfate pentahydrate (1 g) were added to the alkaline solution. The mixture was magnetically stirred for 60 min and then transferred to a 100 mL bottle. The bottle was sealed and placed in oven at 120°C for 24 h. After this time, the bottle was opened. The supernatant was discarded and the settled solid was washed four times with deionized water. The residual solid was dried in oven (120°C) for 24 h. The product was completely powdered in mortar and characterized using SEM (LEO 1455VP scanning microscope), FTIR (Perkin-Elmer spectrophotometer spectrum one) and XRD (Siemens D-5000 diffractometer with Cu K_α radiation).

2.3. Dye removal

Dye adsorption was carried out by mixing 250 mL of dye solution with the adsorbent for 1 h. In certain time intervals, solutions were sampled and the samples were centrifuged at 4,000 rpm. Absorbance of these samples was measured by UV–Vis Spectrophotometer (Perkin-Elmer Lambda 25 Spectrophotometer). Maximum wavelength of BR18 and BB41 were 488 and 580 nm, respectively. The effects of different adsorbent dosages (0.1–1.2 g/L) and initial dye concentrations (20–80 mg/L) on dye removal from wastewater were investigated at 25°C for 1 h.

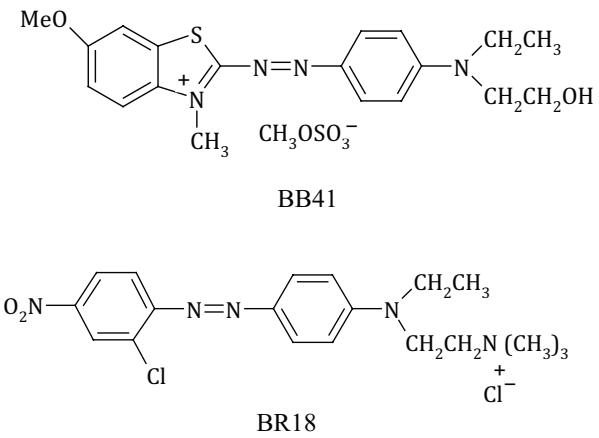

Fig. 1. The chemical structure of dyes.

3. Results and discussion

3.1. Modeling of dye removal using ANFIS

ANFIS can be defined as a type of artificial neural network which is based on Takagi–Sugeno fuzzy inference system. ANFIS is a combination of artificial neural network and fuzzy logic. Therefore, it potentially benefits from the merits of both. ANFIS divides the input space into several neighborhoods that each of them is a fuzzy membership function. Based on given data, ANFIS generates either linear or constant value rules to minimize the error. Fuzziness of the neighborhoods allows a flexible interpolation between the given rules. ANFIS has been applied in some researches in field of adsorption process and appropriate results were obtained [29]. More detailed information about ANFIS can be found in another paper [30]. In this study, 70 experimental data sets were obtained for each dye from laboratory. 70% of data sets were used for training and the else used for testing.

In order to have similar domains, all data were normalized between 0.2 and 0.8. The modeling was done in MATLAB R2008a environment. For modeling of adsorption process using ANFIS, first, fuzzy inference system structure was generated from data through grid partition. Different topologies with various types, numbers of membership functions related to inputs and types of functions that were used for output, were investigated. Table 1 presents the values or types of changeable ANFIS parameters that were used for optimization of the ANFIS model. All possible conditions (540 conditions for each dye) were studied.

It should be mentioned that the hybrid method was considered as optimization method which was applied in membership function parameter training. The hybrid

Table 1
The values or types of changeable parameters of ANFIS

Specification	Ranges or types
Number of membership functions associated with input 1 (time)	2–6
Number of membership functions associated with input 2 (dye concentration)	2–4
Number of membership functions associated with input 3 (adsorbent amount)	2–4
Type of membership functions associated with inputs	Gaussmf, gbellmf, gauss2mf, pimf, dsigmf, psigmf
Type of function associated with output	Constant or linear

method was combination of least squares estimation with backpropagation.

The performance of modeling was investigated using graphical plots and statistical parameters, coefficient of determination (R^2) and mean squared error (MSE), which are defined as:

$$R^2 = 1 - \frac{\sum_{i=1}^{N}(y_{i,\text{pred}} - y_{i,\text{exp}})^2}{\sum_{i=1}^{N}(y_{i,\text{exp}} - \overline{y}_{\text{exp}})^2} \quad (1)$$

$$\text{MSE} = \frac{1}{N}\sum_{i=1}^{N}\left(y_{i,\text{pred}} - y_{i,\text{exp}}\right)^2 \quad (2)$$

The model which had the lowest MSE for test data was selected as the optimum model. The specifications of the optimum models and the architectures of them are presented in Table 2 and Fig. 2, respectively.

Fig. 4 presents the ANFIS predicted dye removal percentage vs. experimental values. As shown in this figure, all data were distributed well around diagonal line, which means the predicted and experimental values are similar to a large extent. As a result, based on graphical plots, values of R^2 which are close to 1 and the low values of MSE, ANFIS is suggested as a powerful tool for modeling of adsorption process.

3.2. Effect of operational parameters on dye removal

Fig. 5 shows the values of dye removal percentage at different $CuMnO_2$ dosages. The increase in dye removal percentage with increasing the amount of adsorbent can be attributed to the increased adsorbent surface area and availability of larger number of adsorption sites. However, the adsorption capacity (which is expressed in milligram adsorbed per gram of the adsorbent) decreased with

Table 2
The specifications of the optimum models

Specification	BB41	BR18
Number of membership functions associated with input 1 (time)	2	2
Number of membership functions associated with input 2 (concentration)	3	2
Number of membership functions associated with input 3 (adsorbent amount)	2	4
Type of membership functions associated with inputs (Fig. 3)	gaussmf	gauss2mf
Type of function associated with output	Linear	Linear
R^2 testing	0.9977	0.9922
R^2 training	0.9996	0.9971
MSE testing[a]	3.80E–05	7.60E–05
MSE training[a]	8.51E–06	3.38E–05

[a]The values of these parameters were calculated using normalized data.

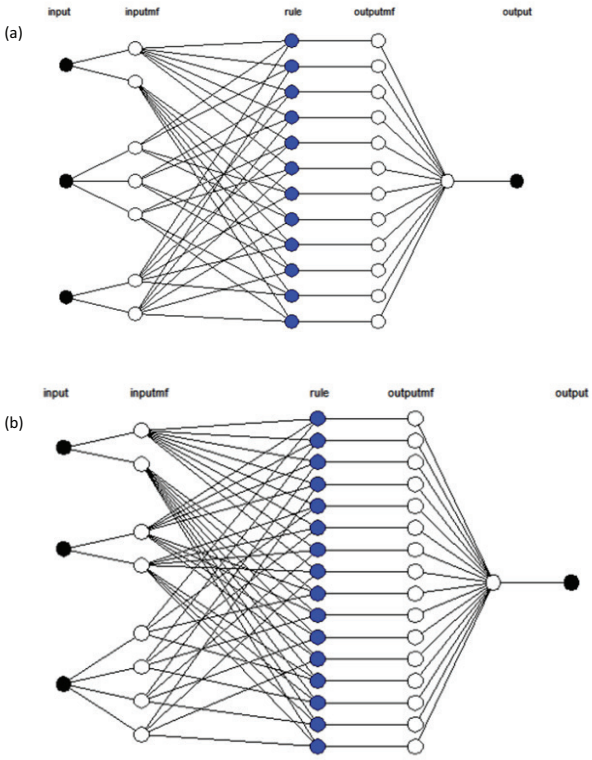

Fig. 2. The architecture of optimum model for (a) BB41 and (b) BR18.

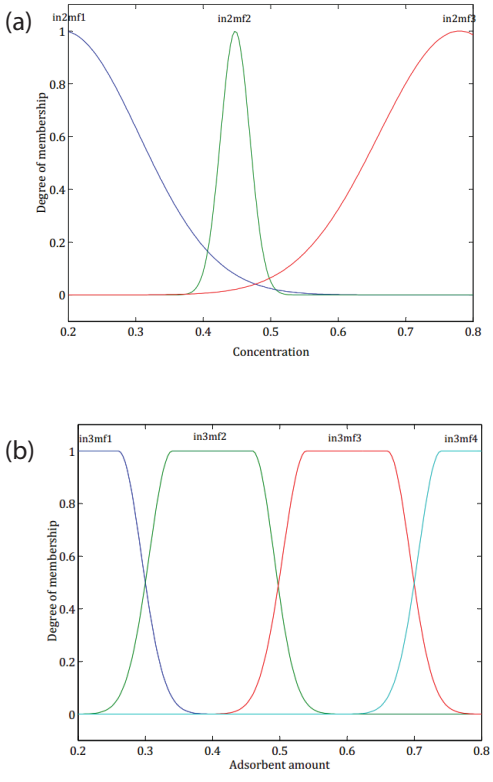

Fig. 3. Sample of membership functions associated with inputs (a) BB41 and (b) BR18.

increasing the amount of the adsorbent. It was due to the overlapping or aggregation of adsorption sites, resulting in a decrease in total adsorbent surface area available to the dye and an increase in diffusion path length [31].

Fig. 6 indicates the effect of initial dye concentration on dye adsorption. Experiments were conducted at different dye concentrations (20–80 mg/L). For both pollutants, the values of dye removal percentage decreased by increasing the initial concentrations. This trend is probably due to the saturation of the active binding sites on the adsorbent surface at higher dye concentrations [19].

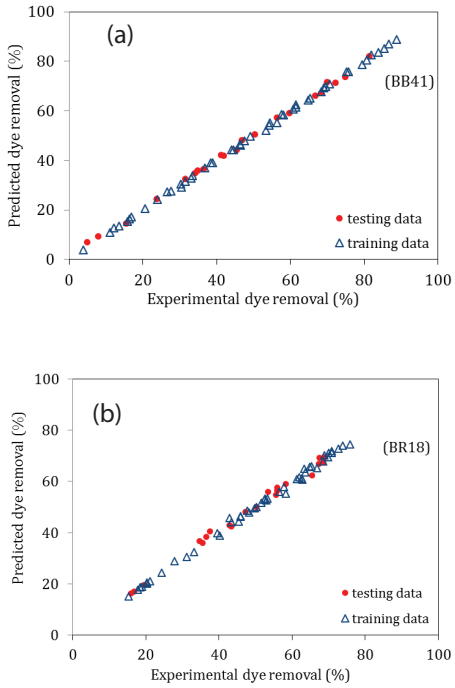

Fig. 4. ANFIS predicted dye removal percentage vs. experimental dye removal values.

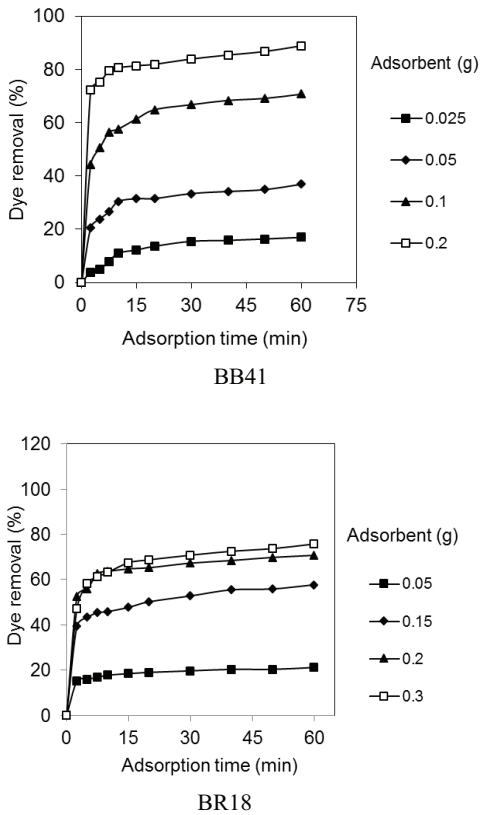

Fig. 5. The effect of adsorbent dosage on dye removal.

3.3. Adsorption kinetics and isotherm

The kinetics investigates the mechanism of dye adsorption onto the adsorbent. In this study, the dye adsorption kinetics on $CuMnO_2$ was studied using pseudo-first-order, pseudo-second-order and intraparticle diffusion models.

The linear plots of $\log(q_e - q_t)$ vs. contact time t (Fig. 7), t/q_t vs. t (Fig. 8) and q_t vs. $t^{1/2}$ (Fig. 9) for dye removal by $CuMnO_2$ nanomaterial at different adsorbent dosages were plotted. The values of k_1, k_2, k_p, R^2, I, and the calculated q_e ($(q_e)_{cal}$) are shown in Table 3.

The R^2 values show that dye adsorption by $CuMnO_2$ nanomaterial did not fit the pseudo-first-order and intraparticle diffusion kinetics. The dye removal kinetics followed pseudo-second-order model due to the linearity between the t/q_t and t.

Adsorption isotherm studies the relation between the mass of dye adsorbed at constant temperature per unit mass of adsorbent and dye concentration of liquid phase at equilibrium. In this study, several isotherms including Langmuir, Freundlich and Temkin models were investigated in detail and the values of isotherm constants are shown in Table 4.

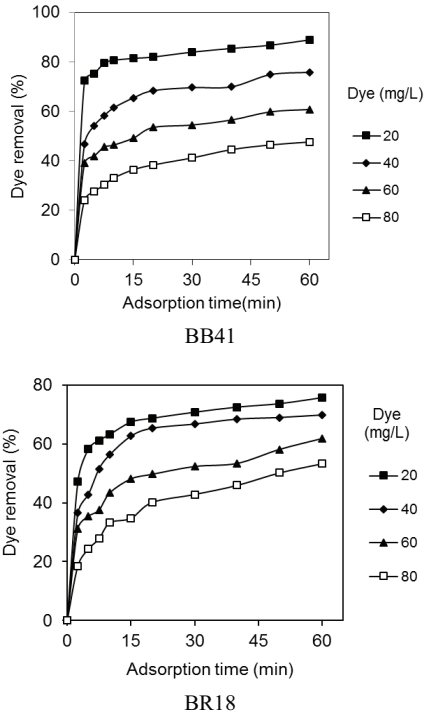

Fig. 6. The effect of dye concentration on dye removal.

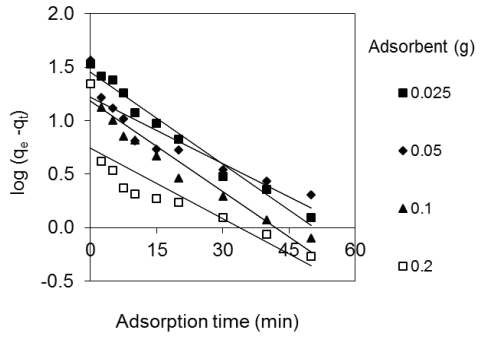

BB41

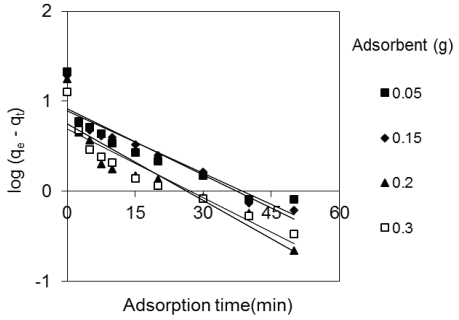

BR18

Fig. 7. The pseudo-first-order kinetics of dye removal.

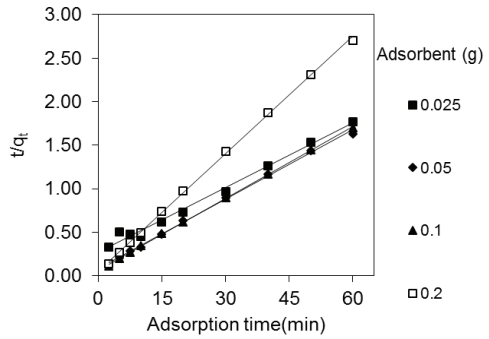

BB41

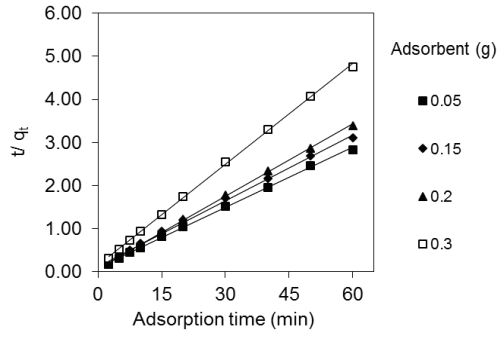

BR18

Fig. 8. The pseudo-second-order kinetics of dye removal.

The R^2 values show that the dye removal isotherm for BB41 and BR18 followed the Langmuir model (Table 4). It means the adsorption of BB41 and BR18 occurred at specific homogeneous sites and a one layer adsorption onto $CuMnO_2$ surface.

3.4. Characterization

FTIR spectrum of $CuMnO_2$ nanomaterial is shown in Fig. 10. The peak at 3,435 cm^{-1} is assigned for O–H stretching. A peak appeared at 1,631.5 cm^{-1} is for O–H bending of molecular water [32]. The band at about 1,384 cm^{-1} is also ascribed to the bending vibrations of the O–H groups combined with manganese oxides [33]. The peak at 1,003 cm^{-1} is assigned to the bending vibration of H_2O and OH, which implies that the hydroxyl groups existed in MnO_2 [34]. Also, the peak at 735 cm^{-1} can be attributed to free nitrate ion [35]. The two peaks at 615 and 511 cm^{-1} can be ascribed to the stretching vibration of the Mn–O and Mn–O–Mn bands [34,36].

The morphology and structure of $CuMnO_2$ nanomaterial were investigated by SEM (Fig. 11). The SEM images show the flake shape of the adsorbent. Based on the images, it is clear that the adsorbent particles are nanosized.

Fig. 12 illustrated the XRD pattern of the synthesized adsorbent. The peaks are matched well with the peaks of the $CuMnO_2$ reported in the previous published paper [32].

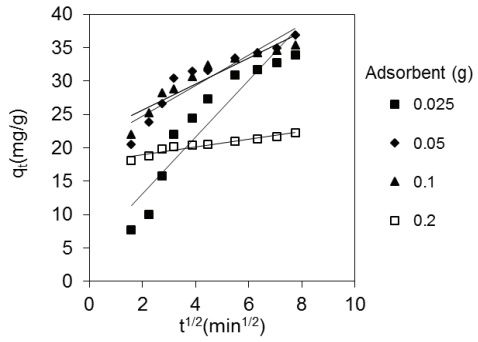

BB41

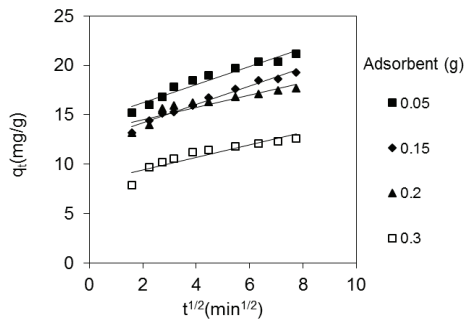

BR18

Fig. 9. The intraparticle diffusion kinetics of dye removal.

Table 3
The linearized kinetics coefficients of dye removal using $CuMnO_2$ at different adsorbent dosages

Dye	Adsorbent (g)	$(q_e)_{exp}$	Pseudo-first-order $\log(q_e - q_t) = \log(q_e) - (k_1/2.303)$			Pseudo-second-order $t/q_t = 1/k_2 q_e^2 + (1/q_e)\, t$			Intraparticle diffusion $q_t = k_p\, t^{1/2} + I$		
			$(q_e)_{cal}$	k_1	R^2	$(q_e)_{cal}$	k_2	R^2	k_p	I	R^2
BB41	0.025	33.92	28.65	0.0663	0.9780	40.49	0.0023	0.9909	4.2460	4.66	0.8815
	0.05	36.89	16.65	0.0479	0.8345	37.59	0.0089	0.9979	2.2791	20.19	0.8647
	0.1	35.35	15.32	0.0654	0.9090	36.36	0.0119	0.9996	1.9436	21.80	0.8814
	0.2	22.21	5.50	0.0507	0.7121	22.27	0.0383	0.9993	0.5754	17.82	0.9203
BR18	0.05	21.20	7.79	0.0532	0.8330	21.46	0.0231	0.9989	0.9220	14.39	0.9493
	0.15	19.26	8.28	0.0564	0.8910	19.69	0.0199	0.9981	0.9402	12.28	0.9778
	0.2	17.69	5.55	0.0649	0.8377	17.92	0.0396	0.9996	0.6327	13.21	0.8365
	0.3	12.63	4.90	0.0585	0.8629	12.87	0.0377	0.9994	0.6269	8.19	0.8456

Table 4
The linearized isotherm coefficients of dye removal using $CuMnO_2$ at different adsorbent dosages

Langmuir $C_e/q_e = 1/K_L Q_0 + C_e/Q_0$			Freundlich $\log q_e = \log K_F + (1/n)\log C_e$			Temkin $q_e = B_1 \ln K_T + B_1 \ln C_e$		
Q_0	K_L	R^2	K_F	$1/n$	R^2	K_T	B_1	R^2
BB41								
37.17	1.1645	0.9857	20.35	0.2206	0.7142	23.99	6.22	0.7002
BR18								
27.32	0.2370	0.9526	8.23	0.3633	0.7049	2.25	6.16	0.7650

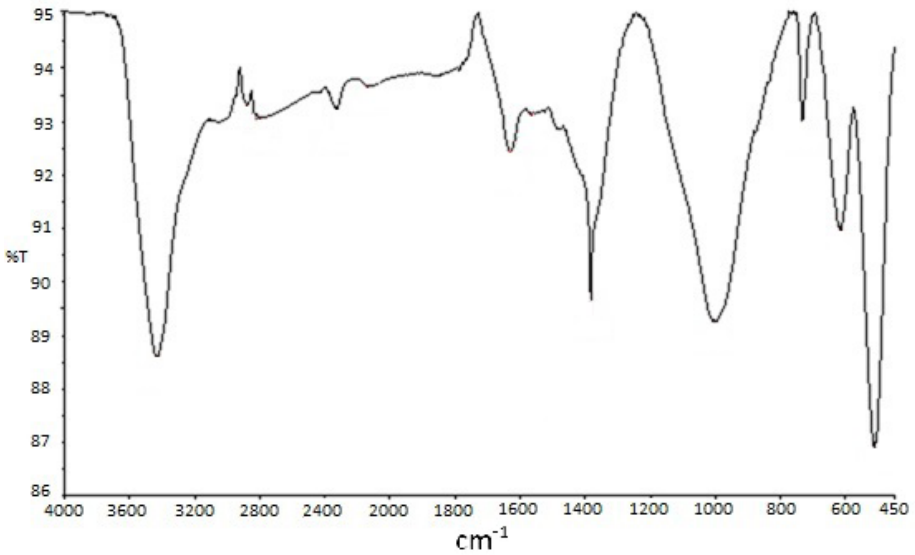

Fig. 10. Fourier transform infrared (FTIR) spectrum of $CuMnO_2$.

4. Conclusion

In this paper, $CuMnO_2$ nanomaterial was synthesized, characterized and used to remove cationic dyes (BR18 and BB41) from wastewater. Dye removal process was modeled using ANFIS. The adsorption kinetics and isotherm followed the pseudo-second-order model and the Langmuir isotherm model, respectively. Moreover, superiority and precision of the dye adsorption modeling using ANFIS were proven. The results showed that $CuMnO_2$ nanomaterial could be used as a suitable adsorbent for cationic dye removal from wastewater.

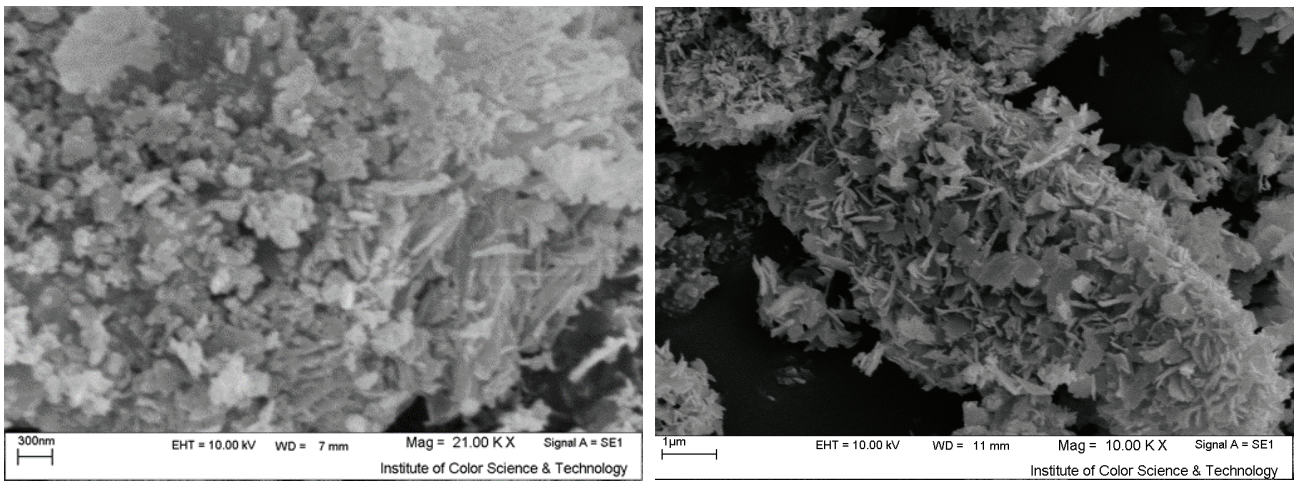

Fig. 11. Scanning electron microscopy (SEM) image of $CuMnO_2$.

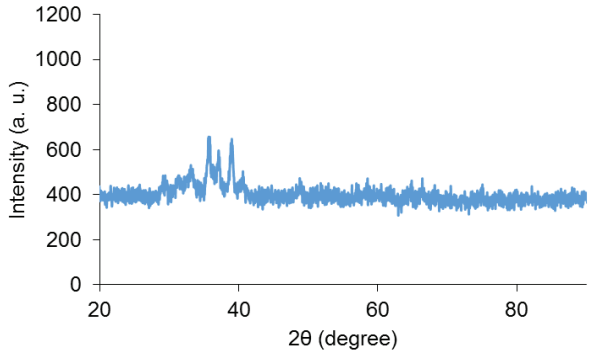

Fig. 12. X-ray diffraction (XRD) pattern of $CuMnO_2$.

Symbols

q_e	—	Adsorbed dye onto adsorbent at equilibrium, mg/g
q_t	—	Amount of adsorbed dye onto adsorbent at time t, mg/g
k_1	—	Equilibrium rate constant of pseudo-first-order kinetics, 1/min
k_2	—	Equilibrium rate constant of pseudo-second-order, g/mg min
k_p	—	Intraparticle diffusion rate constant
I	—	Intercept
C_e	—	Equilibrium concentration of dye solution, mg/L
K_L	—	Langmuir constant, L/g
Q_0	—	Maximum adsorption capacity, mg/g
K_F	—	Freundlich constant
$1/n$	—	Adsorption intensity
K_T	—	Equilibrium binding constant, L/mol
N	—	Number of data points
$y_{i,\text{pred}}$ and $y_{i,\text{exp}}$	—	Predicted and experimental y value of point i, respectively
$\bar{y}_{\text{exp}}$	—	Average of experimental values

References

[1] N.M. Mahmoodi, B. Hayati, M. Arami, Kinetic, equilibrium and thermodynamic studies of ternary system dye removal using a biopolymer. Ind. Crops Prod., 35 (2012) 295–301.
[2] N.M. Mahmoodi, F. Najafi, Synthesis, amine functionalization and dye removal ability of titania/silica nano-hybrid, Micropor. Mesopor. Mater., 156 (2012) 153–160.
[3] A. Mittal, R. Ahmad, I. Hasan, Poly (methyl methacrylate)-grafted alginate/Fe_3O_4 nanocomposite: synthesis and its application for the removal of heavy metal ions, Desal. Wat. Treat., 57 (2016) 19820–19833.
[4] N.M. Mahmoodi, N.Y. Limaee, M. Arami, S. Borhany, M. Mohammad-Taheri, Nanophotocatalysis using nanoparticles of titania: mineralization and finite element modelling of Solophenyl dye decolorization, J. Photochem. Photobiol., A, 189 (2007) 1–6.
[5] N.M. Mahmoodi, Z. Hosseinabadi-Farahani, H. Chamani, Synthesis of nanostructured adsorbent and dye adsorption modeling by an intelligent model for multicomponent systems, Korean J. Chem. Eng., 33 (2016) 902–913.
[6] N.M. Mahmoodi, Synthesis of magnetic carbon nanotube and photocatalytic dye degradation ability, Environ. Monit. Assess., 186 (2014) 5595–5604.
[7] N.M. Mahmoodi, Photocatalytic degradation of dyes using carbon nanotube and titania nanoparticle, Water Air Soil Pollut., 224 (2013) 1612.
[8] N.M. Mahmoodi, Dendrimer functionalized nanoarchitecture: synthesis and binary system dye removal, J. Taiwan Inst. Chem. Eng., 45 (2014) 2008–2020.
[9] N.M. Mahmoodi, Nickel ferrite nanoparticle: synthesis, modification by surfactant and dye removal ability, Water Air Soil Pollut., 224 (2013) 1419.
[10] A.A. Azzaz, S. Jellali, A.A. Assadi, L. Bousselmi, Chemical treatment of orange tree sawdust for a cationic dye enhancement removal from aqueous solutions: kinetic, equilibrium and thermodynamic studies, Desal. Wat. Treat., 57 (2016) 22107–22119.
[11] N.M. Mahmoodi, Manganese ferrite nanoparticle: synthesis, characterization, and photocatalytic dye degradation ability, Desal. Wat. Treat., 53 (2015) 84–90.
[12] N.M. Mahmoodi, Photodegradation of dyes using multiwalled carbon nanotube and ferrous ion, J. Environ. Eng., 139 (2013) 1368–1374.
[13] I. Elaissaoui, H. Akrout, L. Bousselmi, Electrochemical degradation of dye on lead dioxide electrodeposited on stainless steel: effect of cyclic voltammetry parameters, Desal. Wat. Treat., 57 (2016) 22120–22132.

[14] E.N. El Qada, S.J. Allen, G.M. Walker, Adsorption of basic dyes from aqueous solution onto activated carbons, Chem. Eng. J., 135 (2008) 174–184.
[15] H. Sun, L. Cao, L. Lu, Magnetite/reduced graphene oxide nanocomposites: one step solvothermal synthesis and use as a novel platform for removal of dye pollutants, Nano Res., 4 (2011) 550–562.
[16] M.T. Yagub, T.K. Sen, S. Afroze, H.M. Ang, Dye and its removal from aqueous solution by adsorption: a review, Adv. Colloid Interface Sci., 209 (2014) 172–184.
[17] N.M. Mahmoodi, Binary catalyst system dye degradation using photocatalysis, Fibers Polym., 15 (2014) 273–280.
[18] X. He, K.B. Male, P.N. Nesterenko, D. Brabazon, B. Paull, J.H. Luong, Adsorption and desorption of methylene blue on porous carbon monoliths and nanocrystalline cellulose, ACS Appl. Mater. Interfaces, 5 (2013) 8796–8804.
[19] N.M. Mahmoodi, Synthesis of core–shell magnetic adsorbent nanoparticle and selectivity analysis for binary system dye removal, J. Ind. Eng. Chem., 20 (2014) 2050–2058.
[20] F.Z. Mahjoubi, A. Khalidi, M. Abdennouri, N. Barka, M-Al-SO_4 layered double hydroxides (M = Zn, Mg or Ni): synthesis, characterization and textile dyes removal efficiency, Desal. Wat. Treat., 57 (2016) 21564–21576.
[21] K. Singh, S. Arora, Removal of synthetic textile dyes from wastewaters: a critical review on present treatment technologies, Crit. Rev. Environ. Sci. Technol., 41 (2011) 807–878.
[22] K. Benmansour, S. Kara Slimane, A. Benosman, Adsorptive removal of Acidol Red 2BE-NW from aqueous solutions using chitosan/montmorillonite beads, Desal. Wat. Treat., 57 (2016) 21071–21082.
[23] A. Mittal, M. Teotia, R. Soni, J. Mittal, Applications of egg shell and egg shell membrane as adsorbents: a review, J. Mol. Liq., 223 (2016) 376–387.
[24] N.M. Mahmoodi, B. Hayati, M. Arami, F. Mazaheri, Single and binary system dye removal from colored textile wastewater by a dendrimer as a polymeric nanoarchitecture: equilibrium and kinetics, J. Chem. Eng. Data, 55 (2010) 4660–4668.
[25] A. Mittal, R. Ahmad, I. Hasan, Iron oxide-impregnated dextrin nanocomposite: synthesis and its application for the biosorption of Cr(VI) ions from aqueous solution, Desal. Wat. Treat., 57 (2016) 15133–15145.
[26] G. Sharma, M. Naushad, D. Pathania, A. Mittal, G. El-Desoky, Modification of *Hibiscus cannabinus* fiber by graft copolymerization: application for dye removal, Desal. Wat. Treat., 54 (2015) 3114–3121.
[27] J. Ma, F. Yu, L. Zhou, L. Jin, M. Yang, J. Luan, Y. Tang, H. Fan, Z. Yuan, J. Chen, Enhanced adsorptive removal of methyl orange and methylene blue from aqueous solution by alkali-activated multiwalled carbon nanotubes, ACS Appl. Mater. Interfaces, 4 (2012) 5749–5760.
[28] N.M. Mahmoodi, Surface modification of magnetic nanoparticle and dye removal from ternary systems, J. Ind. Eng. Chem., 27 (2015) 251–259.
[29] D. Bingöl, M. Inal, S. Çetintaş, Evaluation of copper biosorption onto date palm (*Phoenix dactylifera* L.) seeds with MLR and ANFIS models, Ind. Eng. Chem. Res., 52 (2013) 4429–4435.
[30] J.-S. Jang, ANFIS: adaptive-network-based fuzzy inference system, IEEE Trans. Syst. Man Cybern., 23 (1993) 665–685.
[31] N.M. Mahmoodi, Synthesis of amine-functionalized magnetic ferrite nanoparticle and its dye removal ability, J. Environ. Eng., 139 (2013) 1382–1390.
[32] S.A. Abdel-Hameed, F.H. Margha, A.A. El-Meligi, Investigating hydrogen storage behavior of $CuMnO_2$ glass-ceramic material, Int. J. Energy Res., 38 (2014) 459–465.
[33] R. Chen, J. Yu, W. Xiao, Hierarchically porous MnO_2 microspheres with enhanced adsorption performance, J. Mater. Chem. A, 1 (2013) 11682–11690.
[34] S. Liang, F. Teng, G. Bulgan, R. Zong, Y. Zhu, Effect of phase structure of MnO_2 nanorod catalyst on the activity for CO oxidation, J. Phys. Chem. C, 112 (2008) 5307–5315.
[35] N. Bayal, P. Jeevanandam, Synthesis of CuO@NiO core-shell nanoparticles by homogeneous precipitation method, J. Alloys Compd., 537 (2012) 232–241.
[36] A. Vázquez-Olmos, R. Redón, G. Rodríguez-Gattorno, M.E. Mata-Zamora, F. Morales-Leal, A.L. Fernández-Osorio, J.M. Saniger, One-step synthesis of Mn_3O_4 nanoparticles: structural and magnetic study, J. Colloid Interface Sci., 291 (2005) 175–180.